ADVANCED FUNCTIONAL MATERIALS
www.afm-journal.de

Polyferrocene-Based Cubosomes: Conversion to Magnetic Mesoporous Microparticles, Supramolecular Modification, and Oxidation Response

Chin Ken Wong, Suna Azhdari, Marvin Foith, Chen Chen, and André H. Gröschel**

Polymer cubosomes (PCs) are an emerging class of mesoporous microparticles that are produced through solution self-assembly of highly asymmetric block copolymers (BCPs). They proved useful for encapsulation or templating replicas for catalysis and energy storage. Although PCs made from BCPs with intrinsic functions such as response to stimuli, degradation, or coordination canopen their use for more diverse applications, reports on PCs with innate functions are still rare. Herein, PCs based on organometallic BCPs bearing pendant ferrocene moieties is reported. The poly(ethylene oxide)-*block*-poly(2-(methacryoyloxy)ethyl ferrocene carboxylate) BCPs (PEO_{44}-*b*-$PFcEMA_x$) with highly asymmetric weight fraction is synthesized in favor of the hydrophobic block ($x = 76–245$). Of these, PEO_{44}-*b*-$PFcEMA_{96}$ assembled into PCs with an average particle diameter of 1.82 ± 0.48 µm, a double diamond lattice, and a pore diameter of ≈30–40 nm. The functionality of these PCs are showcased by i) templating metal oxide replica with concurrent decoration of magnetic iron oxide upon calcination, ii) supramolecular modification of the PC wall via host-guest chemistry, and iii) degradation of the PC structure on demand through oxidation. Exploring these and other block chemistries enriches thetoolbox for PC applications and fosters theunderstanding about PCs by identifying differences or communalities in formation mechanisms and particle structure.

1. Introduction

The self-assembly of block copolymers (BCPs) in solution is one of the main sources for highly defined nanoparticles with controlled shapes and dimensions.[1] While spherical micelles, cylinder micelles, and polymersomes have been thoroughly studied over the past decades, more recently,[2,3] asymmetric BCPs with a hydrophobic fraction exceeding 90 wt.% ($f_B \geq 0.9$) were found to self-assemble into microparticles with highly ordered, solvent-filled channel systems, termed polymer cubosomes (PCs) or hexosomes depending on the lattice symmetry.[4–8] PCs thereby feature two interpenetrating bicontinuous channels with mesopores and a large internal surface area, making them excellent candidates for templating and encapsulation.[9–11]

To date, most reported PCs consist of BCPs with a hydrophilic polyethylene oxide (PEO) corona and a hydrophobic polystyrene (PS) wall.[2,3,12–17] The PEO/PS combination is so effective that several variations of polymer architecture have been shown to form cubosomes, including linear PEO-*b*-PS,[3,16,17] branched-linear *b*PEO-*b*-PS,[2,12–14] and bottlebrush PEO-*b*-PNB-*g*-PS (PNB = polynorbornene) polymers.[15] These polymers served very well as template for organic and inorganic replicas including metal–organic[18] and covalent organic frameworks,[19] a range of transition metals[20] and metal oxides[21] some of which could be used further as scaffolds for

C. K. Wong
School of Chemistry
University of New South Wales
Sydney, NSW 2052, Australia
E-mail: c.kenwong@unsw.edu.au

S. Azhdari
Physical Chemistry
University of Münster
Corrensstraße 28–30, 48149 Münster, Germany

M. Foith, A. H. Gröschel
Polymer materials for energy storage
Bavarian Centre for Battery Technology (BayBatt)
University of Bayreuth
95448 Bayreuth, Germany
E-mail: andre.groeschel@uni-bayreuth.de

C. Chen
School of Chemical Engineering
Dalian University of Technology
No.2 Linggong Road, Ganjingzi District, Dalian 116024, China

A. H. Gröschel
Bavarian Polymer Institute (BPI) and Bayreuther Institut für Makromolekülforschung (BIMF)
University of Bayreuth
95447 Bayreuth, Germany

The ORCID identification number(s) for the author(s) of this article can be found under https://doi.org/10.1002/adfm.202522652

DOI: 10.1002/adfm.202522652

conjugated polymers,[22] and mesoporous carbon for application in catalysis[23,24] and energy storage.[25,26] The robust PS lattice thereby typically serves as structure-directing support, while the PEO corona enables the efficient coordination of precursor molecules for subsequent conversion into replicas throughout the entire cubosome channel system.

PCs based on PEO/PS, do, however, not possess any innate function (aside from mechanical stability), and they are thus limited in terms of response to stimuli, degradation, coordination, and so on. This has prompted the exploration of other block chemistries to impart functionality into these structures. An early example used polyacrylic acid (PAA) to confer the pH-responsive properties of PAA onto the surface of the cubosomes channel system.[27] Applying minute changes in pH allowed to manipulate the pore size of the cubosome structure and to control the passage of macromolecules (e.g., proteins) in and out of the system via a pH-gated regulation. Other corona examples include pH-responsive polycationic poly(2vinyl pyridine)[28] and crown-ether modifications to alter corona volume via salt complexation.[29]

Regarding the cubosome wall, only a few functional chemistries were reported, e.g., poly(tetraphenylethylene methacrylate) to introduce aggregation-induced emission during assembly, useful for bioimaging[30] or a copolymer of poly(pentafluorostyrene-*co*-polystyrene) to introduce photo-crosslinkable sites for PC stabilization.[31] Since the wall-forming block is mainly responsible for structural stability, responsive blocks open the possibility for controlled dis-/assembly or degradation. This was demonstrated on BCPs with a PAA block protected with a pinacol boric ester functionality that could be deprotected through oxidation, leading to the transition into a bishydrophilic BCP and the dissolution of the PCs.[32] We recently reported a similar non-reversible transition from an amphiphilic to bishydrophilic BCP, where a photocleavable nitrobenzyl ester moiety could be removed from the walls of the already assembled PCs by a few min of irradiation with sunlight.[33] While these systems aim for a stimuli triggered release of cargo, we recently also reported on the complete biodegradation of the BCP and PC into small molecules for agrochemistry.[34] The PCs consisted of a polyphosphoester corona and a racemic polylactide wall. Loading the hydrophobic fungicide tebuconazole into the PC wall during assembly allowed application of the mesoporous microparticles on various crops for anti-fungal protection, followed by degradation of the PCs into fertilizer (phosphates).

Aside from stabilization or degradation of the PC structure, functional wall-forming blocks are attractive for the incorporation of reactive sites. In this direction, we synthesized BCPs of PEO-*b*-PAcS (PAcS = poly(4-acetoxystyrene))[35] that add possibilities to customize the polarity and functionality of the PC wall through hydrolysis into poly(4-hydroxystyrene). Using poly(4-vinylpyridine) (P4VP) as PC wall, on the other hand, opened the possibility for the coordination of metals and nanoparticles (e.g., platinum) to produce heterogeneous catalysts.[36] Such PCs could, in principle, be used to create multifunctional materials, where a replica of the channel system is first formed via sol–gel reaction, while a second material is added to the PC wall.

Here, we report on PCs with multifunctional properties that originate from pendant ferrocene moieties of the underlying BCPs (**Figure 1**). The incorporation of this organometallic component[37] in form of poly(2-(methacryloyloxy)ethyl ferrocene carboxylate) (FcEMA) leads to PCs that i) serve as a template to form SiO_2 replica with concurrent deposition of magnetic iron oxide onto the replica upon calcination, ii) undergo supramolecular host-guest complexation with a cyclodextrin derivative to enable labeling/encapsulation, and iii) gradually fall apart over time upon exposure to an oxidizing agent that converts amphiphilic PEO-*b*-FcEMA to bishydrophilic PEO-*b*-Fc^+EMA.

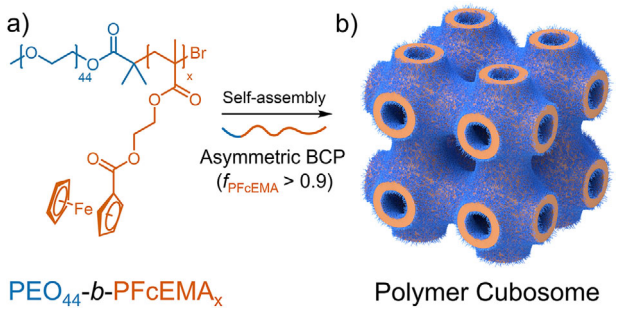

Figure 1. PEO_{44}-*b*-$PFcEMA_x$ BCP used in this study and self-assembly to PCs.

2. Results and Discussion

2.1. BCP Synthesis and Characterization

Ferrocene-bearing PEO-*b*-PFcEMA BCPs were synthesized by atom transfer radical polymerization (ATRP). The synthesis is described here briefly for the composition PEO_{44}-*b*-$PFcEMA_{96}$ featuring asymmetric weight fractions of f_{PEO} = 0.06 and f_{PFcEMA} = 0.94, a number average molecular weight of $M_{n,NMR}$ = 35 000 g mol^{-1}, and a dispersity of $Đ$ = 1.13 (**Figure 2**). First, the FcEMA monomer was synthesized following a literature procedure which involved the esterification of 2-hydroxyethyl methacrylate (HEMA) with ferrocene carboxylic acid (Figure S1, Supporting Information).[38] After screening various polymerization conditions, the best results for ATRP of FcEMA were obtained in dioxane at 70 °C using a PEO_{44}-Br macroinitiator (MI), CuBr, and PMDETA in molar ratios of [MI]:[Cu]:[L] = 1:1.5:3. For $PFcEMA_{96}$, the FcEMA to MI ratio was set to [M]:[MI] = 300:1 and polymerization was allowed to proceed for 8 h to reach a conversion of 30% (Figure 2a). ^{1}H-NMR confirmed the presence of peaks for both blocks, whereas the integrals at δ_b = 3.6 ppm and δ_e = 4.8 ppm were used to calculate the final block compositions for each BCP (Figure 2b). Other PEO_{44}-*b*-$PFcEMA_x$ BCPs were synthesized accordingly, but with varying [M]:[MI] ratio (for details see SI and results Table 1). Controlled polymerization conditions were confirmed by pseudo first-order polymerization kinetics that showed a linear correlation between monomer consumption and time (Figure 2c). The absence of coupling or transfer reactions was confirmed by a linear increase of M_n with conversion and overall low dispersity below 1.3 (Figure 2d). Full initiation was confirmed by GPC, which showed a complete shift of the trace from MI at t = 0 h to BCP already at t = 1 h, without any remaining signal at the molecular weight of the MI (Figure 2e).

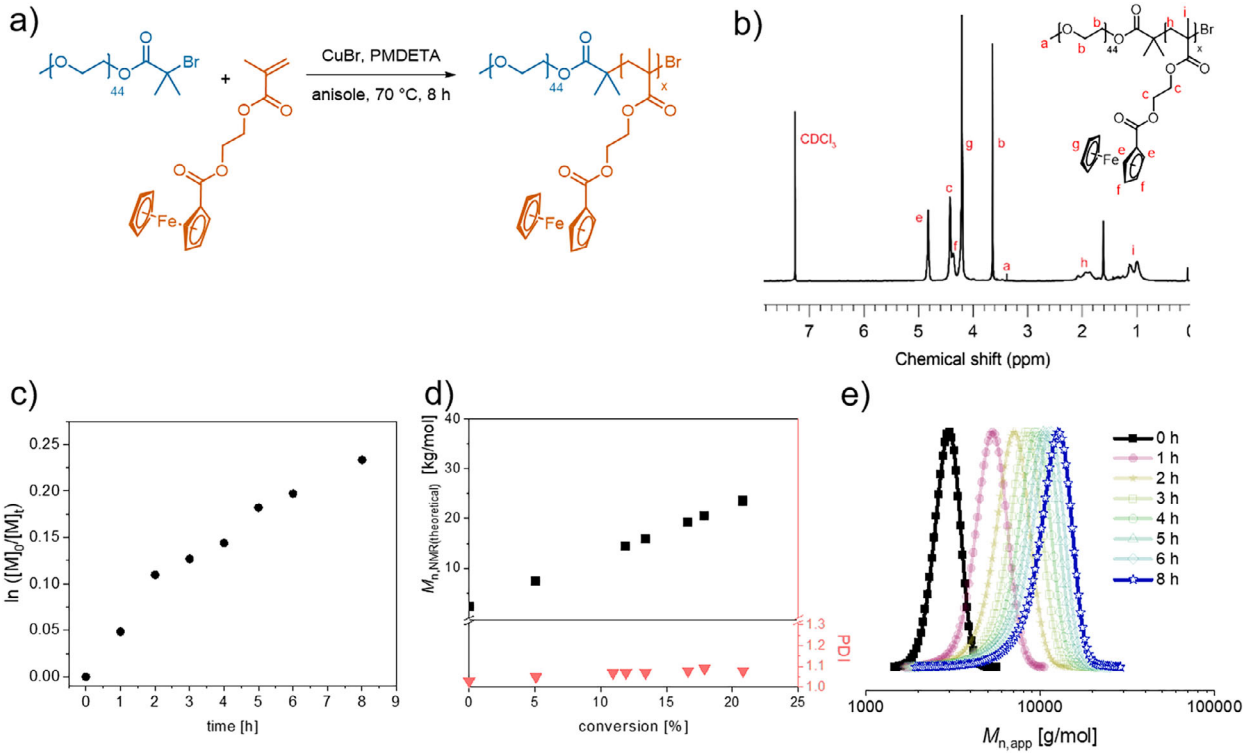

Figure 2. Synthesis of PEO_{44}-*b*-$PFcEMA_{96}$. a) Polymerization conditions. b) ^{1}H-NMR of a purified BCP. c) Linear correlation of monomer consumption over time with pseudo first-order kinetics, and d) linear increase of M_n with conversion and narrow dispersity. e) GPC traces from MI to BCPs.

2.2. Self-Assembly and Characterization of PCs

The formation of PEO-*b*-PFcEMA PCs and their characterization are summarized in **Figure 3**. In the search for PCs with high-quality structure, we screened several assembly conditions, including block composition, polymer concentration, type of non-solvent, addition rate of non-solvent, and so on, because slight differences in block polarity may impact assembly kinetics at such high hydrophobic weight fractions. Although liquid–liquid phase separation (LLPS)[39] via nanoprecipitation is believed to be one of the typical routes for PC formation,[33] this method did not lead to defined particles for any of the PEO-*b*-PFcEMA compositions, irrespective of the rate of non-solvent addition. Instead, we observed fast sedimentation into undefined aggregates (Figure S2, Supporting Information), which likely originated from the high density of the organometallic moiety (δ_{Fc} = 1.5 g cm^{-3}) as compared to the density of typically used blocks (e.g., PS, PMMA, or P4VP with δ = 1.0–1.2 g cm^{-3}). Surprisingly, the best results were obtained by straightforward dialysis of a 10 g L^{-1} solution of PEO-*b*-PFcEMA from THF into water, whereas dioxane merely led to closed spheres (Figure S3, Supporting Information) and a 20 g L^{-1} solution to additional side morphologies (Figure S4, Supporting Information). During dialysis, the slow influx of water into the dialysis bag gradually exposes the molecularly dissolved PEO-*b*-PFcEMA to water, providing a more gentle transition into the LLPS regime. This transition is coupled to the onset of self-assembly of the PFcEMA block within the polymer-rich droplets, while amphiphilicity and high asymmetry of the BCP both determine the bicontinuous morphology. Using dialysis, all PEO_{44}-*b*-$PFcEMA_x$ formed microparticles under the above-mentioned conditions (Figure S5, Supporting Information). However, only BCPs with a length of $PFcEMA_{76\text{-}96}$ formed cubosomes, whereas $PFcEMA_{182\text{-}196}$ lead a mixture of cubosomes and hexosomes, $PFcEMA_{218\text{-}245}$ predominantly

Table 1. PEO_{44}-*b*-$PFcEMA_x$ BCPs with different hydrophobic weight fractions of the PFcEMA block (f_{PFcEMA}).

Sample ID	DP_{FcEMA} [a]	f_{PFcEMA} [b]	$M_{n,\,NMR}$ [c]	$Đ$ [d]
PEO_{44}-*b*-$PFcEMA_{76}$	76	93.4	28100	1.10
PEO_{44}-*b*-$PFcEMA_{96}$	96	94.3	35000	1.11
PEO_{44}-*b*-$PFcEMA_{182}$	182	97.0	64400	1.15
PEO_{44}-*b*-$PFcEMA_{195}$	195	97.1	68800	1.12
PEO_{44}-*b*-$PFcEMA_{211}$	211	97.2	72200	1.25
PEO_{44}-*b*-$PFcEMA_{218}$	218	97.3	74600	1.14
PEO_{44}-*b*-$PFcEMA_{226}$	226	97.4	77300	1.26
PEO_{44}-*b*-$PFcEMA_{245}$	245	97.7	85900	1.11

[a] Degree of polymerization determined by a combination of GPC and ^{1}H-NMR. [b] Weight fraction of the hydrophobic block; [c] Molecular weight calculated via ^{1}H-NMR; [d] Dispersity determined with GPC using THF as eluent and PS standards.

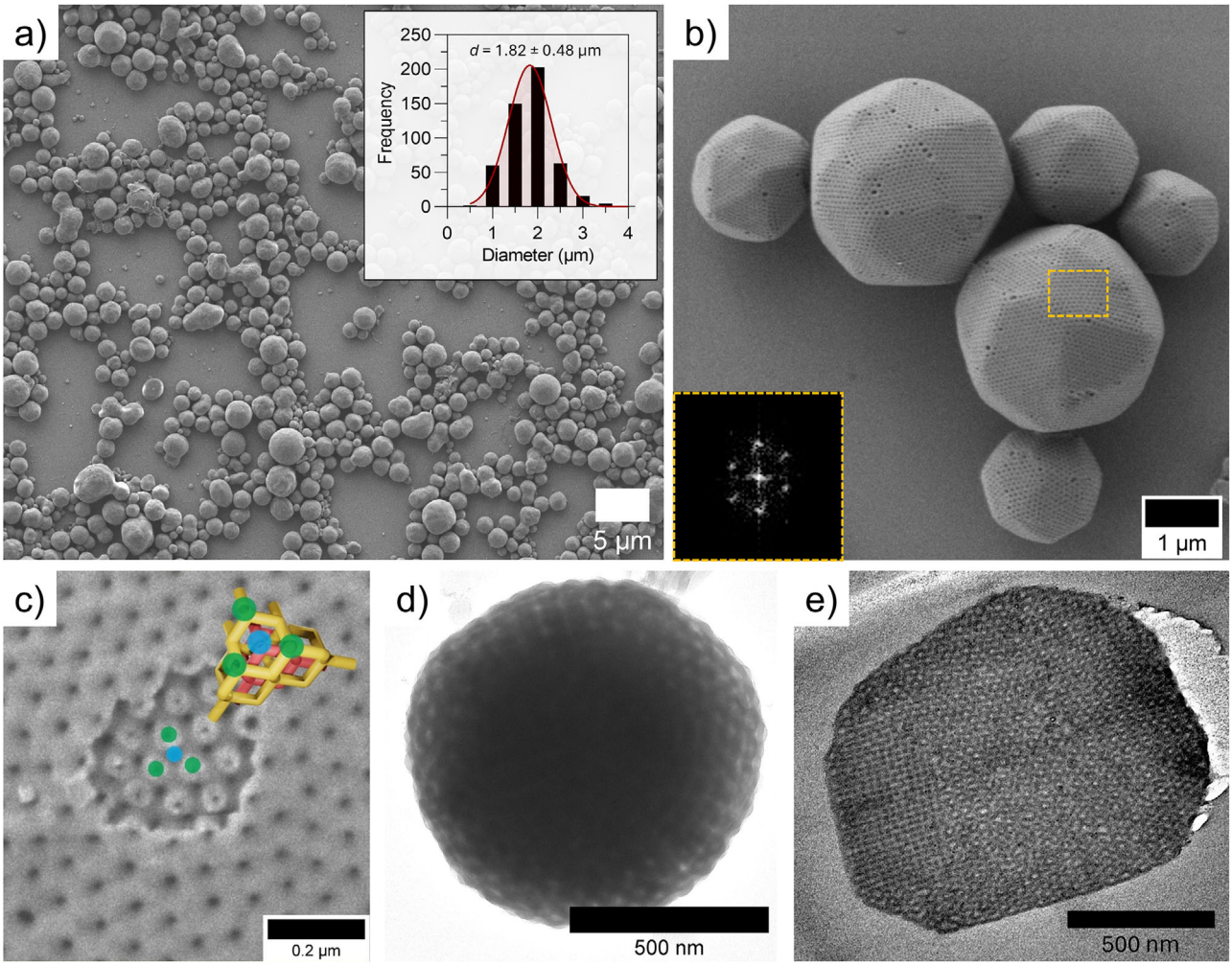

Figure 3. Structural properties of PCs of PEO_{44}-*b*-$PFcEMA_{96}$. a) SEM overview image of mesoporous microparticles. The inset shows a representative size histogram ($n = 500$) based on SEM image analysis. b) Close-up of PCs and FFT image of the yellow outlined region. c) SEM of cracked PC with a *Pn3m* internal structure as indicated in the cartoon. d) TEM image and e) TEM cross-section.

formed hexosomes, and $PFcEMA_{245}$ merely closed spheres without noticeable porosity. This trend of morphological transitions was previously reported also for PCs of PEO-*b*-PS and is associated to the larger required volume of the hydrophobic block within the PC wall.[3] Exemplified on PEO_{44}-*b*-$PFcEMA_{96}$, we obtained PCs with an average particle diameter (d) of 1.82 ± 0.48 µm (Figure 3a) and a relatively narrow size-distribution. Notably, the sample solely consisted of microparticles and did not contain any side morphologies such as polymersomes or cylinder micelles. The PCs exhibit a porous surface and are slightly faceted, which is an indication for a double-diamond lattice (*Pn3m*) with high inner order (Figure 3b). Fast Fourier transformation (FFT) analysis revealed a hexagonal pore arrangement (inset in Figure 3b), while a fractured PC confirmed the *Pn3m* lattice structure (Figure 3c; Figure S6, Supporting Information). The pore-to-pore distance was measured at 60 nm with pore sizes of ≈30–40 nm. TEM imaging confirmed that the porous structure exists throughout the microparticles (Figure 3d), whereas a high inner order could be visualized on ultra-thin cross-sections of embedded microparticles (Figure 3e).

2.3. Sacrificial Templating with Concurrent Iron Oxide Deposition

Having clarified the formation of ferrocene-containing PCs, we sought to utilize the multifunctional properties of ferrocene. For instance, ferrocene can act as a precursor for the synthesis of iron oxide nanoparticles,[40,41] which involves the thermal decomposition of ferrocene (>500 °C in air) into iron atoms that eventually coalesce into iron oxide nanoparticles. Here, we demonstrate that our ferrocene-containing PCs can serve as a sacrificial template for the synthesis of a single diamond (*Fd3m*) inorganic skeletal replica and enable the concurrent deposition of iron oxide nanoparticles (**Figure 4**). It was demonstrated before that only one channel of the double diamond network of *Pn3m* cubosomes is accessible through its surface pores.[14,42] Figure 4a shows a cartoon of a double diamond network, where only the red channel is connected to a porous cubosome surface (and hence "open" to the surrounding solution), while the yellow channel remains segregated or "closed" from the surrounding solution. Incubation of our PCs with a TEOS sol (SiO_2 precursor), therefore, backfills only the red open channel, which should result in

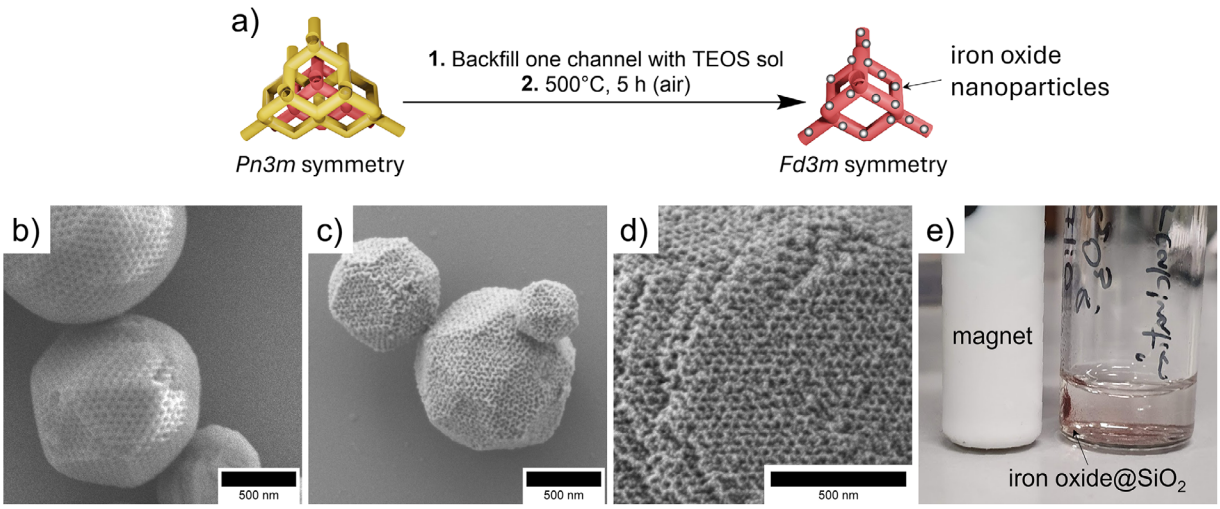

Figure 4. Conversion of PCs to magnetic nanocomposites. a) Cartoon representation and SEM images of b) SiO_2-impregnated PEO_{44}-*b*-$PFcEMA_{96}$ cubosomes with *Pn3m* internal symmetry and c) iron oxide@SiO_2 composites with *Fd3m* internal symmetry formed by first backfilling one open channel of the double diamond network with TEOS sol followed by calcination at 500 °C for 5 h in air. d) High-magnification SEM image showing the deposition <10 nm iron oxide nanoparticles (bright dots) in the SiO_2 replica. e) Photograph highlighting the magnetic attraction of iron oxide@SiO_2 composites towards a weak magnet.

a replica with *Fd3m* symmetry. Subsequent gelation of the TEOS sol via acidification led to the formation of a SiO_2 network selectively within the "red" channel. To remove the cubosome template and initiate iron oxide deposition, we subjected the SiO_2-impregnated cubosomes (Figure 4b) to calcination at 500 °C in air for 5 h. This process thermally decomposes the PC template, leaving behind only the SiO_2 network (SEM image in Figure 4c) bearing the original symmetry of the red channel. The concurrent deposition of <10 nm iron oxide nanoparticles during the calcination process was confirmed by high-magnification SEM (Figure 4d), visible as small bright spots. Due to the presence of the iron oxide nanoparticles, the iron oxide@SiO_2 composites exhibit magnetism and can be isolated from solution using a common magnetic stir bar (Figure 4e). As mentioned in the introduction, PCs can serve as a template for a large range of metal oxides, metals, MOFs/COFs, and carbon (amongst others). Adding magnetic properties to such mesoporous microparticles through the PFcEMA chemistry would allow combining straightforward extraction of PCs after filtration or heterogeneous catalysis.

2.4. Host-Guest-Complexation

Aside from conversion to magnetic iron oxide, ferrocene is also known to form host-guest inclusion complexes with *β*-cyclodextrin (*β*CD) through non-covalent (supramolecular) interactions in water.[43–46] This property makes ferrocene moieties an attractive site for versatile modification, and we sought the possibility of performing supramolecular complexation to our PFcEMA cubosomes (**Figure 5**). For this purpose, we used a model *β*CD derivative labelled with the fluorescent dye, Rhodamine B (RhoB-*β*CD; see chemical structure in Figure S7, Supporting Information).[47] To generate the inclusion complex within the hydrophobic domain of the PCs, we simply added 10 mol% of RhoB-*β*CD (relative to FcEMA) to a PEO_{44}-*b*-$PFcEMA_{96}$ solution before self-assembly through dialysis into water. Excess RhoB-*β*CD that did not form an inclusion complex was removed during the dialysis process. Successful complexation was verified by fluorescence spectroscopy (Figure 5b), which showed a peak centered at ≈575 nm corresponding to the fluorescence maxima of RhoB-*β*CD. Using the calibration curve shown in the inset of Figure 5b, we estimate a complexation efficiency of 15.5%. SEM verified that the added RhoB-*β*CD did not interfere with the self-assembly process and that PCs retained their original structure (Figure 5c; Figure S8, Supporting Information). Fluorescence microscopy confirmed the co-localization of RhoB-*β*CD and the PCs in the fluorescence image and an overlay with a bright field image (Figure 5d,e). There, the fluorescence signal primarily coincides with the location of the microparticles and cannot be detected in the background solution, confirming that the fluorescent dye underwent host-guest complexation in a highly specific manner. Considering the wealth of modified CDs, this would allow the inclusion of a large variety of functionalities within the PC wall.

2.5. Oxidation Response

Ferrocene is redox-active and can be oxidized into a hydrophilic ferrocenium ion, thereby inducing a transition from amphiphilic to bishydrophilic BCP, accompanied by dissolution of the PCs (as well as release of any complexes) (**Figure 6**).[46,48] We envisaged that the redox properties would be conferred into our cubosomes since PFcEMA constitutes a large fraction (f_{PFcEMA} = 0.94) of the structure (Figure 6a). To test this hypothesis, we introduced 0.5 mL of a 100 mM hydrogen peroxide (H_2O_2) solution to 0.5 mL of a PC dispersion with a concentration of 10 mg mL^{-1} and followed the oxidation process for 14 days. We started by

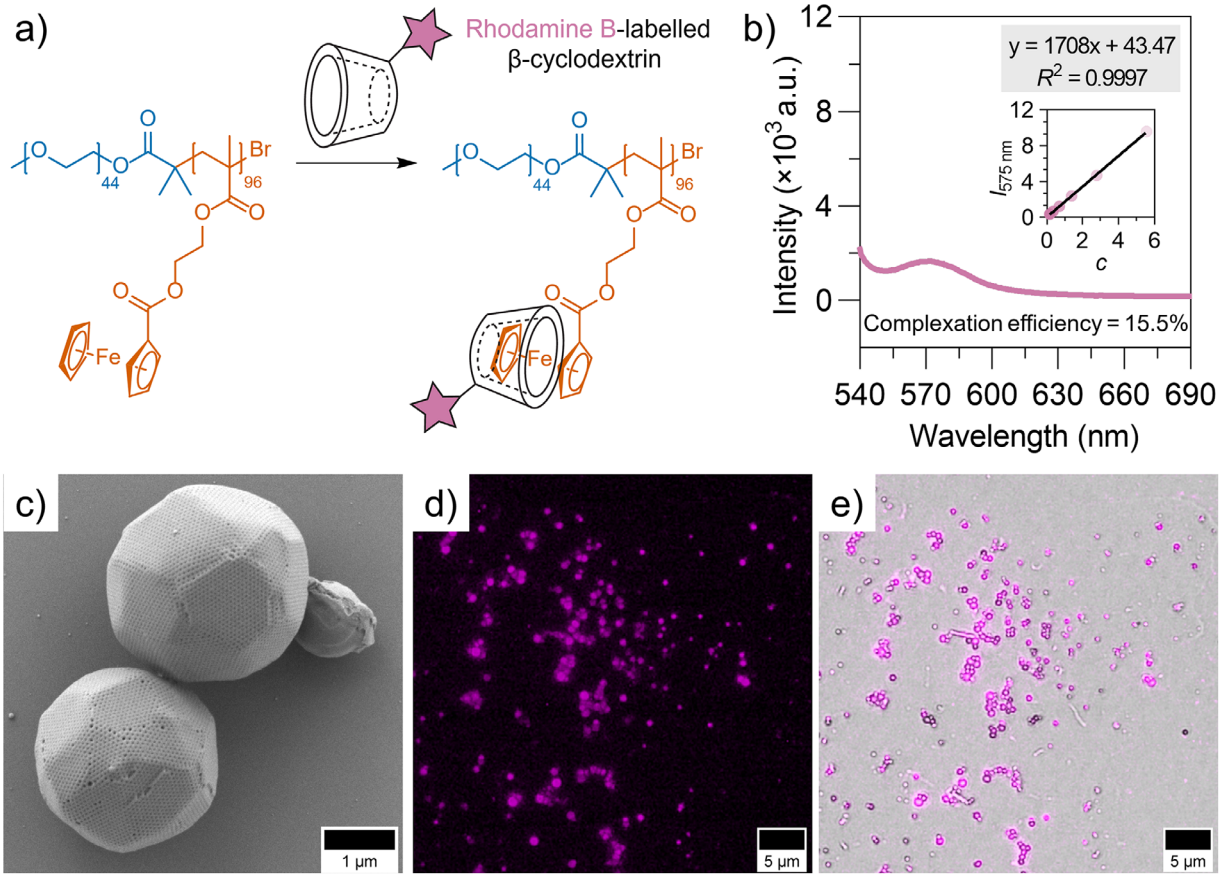

Figure 5. PEO_{44}-*b*-$PFcEMA_{96}$ cubosomes complexed with 10 mol% of RhoB-βCD. a) Ferrocene moieties on PEO_{44}-*b*-$PFcEMA_{96}$ can form inclusion complexes with βCD via supramolecular interactions. b) Fluorescence spectrum with loading efficiency determined through a calibration curve in the inset. c) SEM image of RhoB-modified PC. d) Fluorescence image and e) overlay with brightfield image.

monitoring turbidity changes in the sample using UV–vis spectroscopy (Figure 6b). A minor increase in turbidity was initially observed immediately after H_2O_2-addition, but this gradually reduced over the next 14 days. This data suggested that the cubosomes had indeed undergone an oxidation reaction in the presence of H_2O_2. In order to understand how the morphology of the cubosomes was affected by ferrocene oxidation, we removed aliquots of the sample at different oxidation times and analyzed changes to the cubosome morphology by SEM (Figure 6c). On day 0 (immediately after the addition of H_2O_2), most cubosomes retained their structural integrity. Image analysis, however, indicates an expansion in pore size from ≈30–40 to ≈50–60 nm (compare pores in Figure 3c). We attribute this increase to the swelling of the cubosomes' hydrophobic domain as the hydrophobic ferrocene moieties began to be oxidized into hydrophilic ferrocenium ions on the molecular level. As the oxidation process progressed, we observed the formation of pronounced cracks and onset of deformation in the PCs (day 1) and gradual dissociation of the PCs (days 2, 8, and 14), consistent with the decrease in turbidity. We note here that despite the long oxidation duration (14 days) and bishydrophilic nature of the oxidized polymer, the cubosomes do not completely dissociate into a molecularly dissolved state. The long oxidation times are caused by the initially very hydrophobic PFcEMA domain, which slows down the oxidation process. Copolymerization with a small amount of hydrophilic comonomer (e.g., 5–10 mol% PEGMA) may allow for swelling of the PC wall, faster access of the ferrocene units for the oxidant, and accelerated dissolution.

3. Conclusion

In summary, we reported the preparation of ferrocene-based PCs from asymmetric BCPs of PEO-*b*-$PFcEMA_x$. The ferrocene constituents thereby equip the PCs with diverse functionality. First, they can serve as a sacrificial template that concurrently deposits iron oxide nanoparticles onto an internalized inorganic scaffold upon thermal decomposition, which can be combined with a large variety of metal and metal oxide replicas.[21] These are relevant for catalytic and energy applications. Second, their structure can be modified on the molecular level via supramolecular complexation with βCD derivatives (e.g., dye/drug conjugates), opening the possibility of their use in biomedical applications. Finally, they are oxidation-responsive and can be triggered to decompose in the presence of an oxidant such as H_2O_2, potentially also milder oxidation agents. The possibility to reverse assembly into polymer cubosomes via reduction reactions may help to better understand the still unclear self-assembly mechnism of polymer cubosomes.

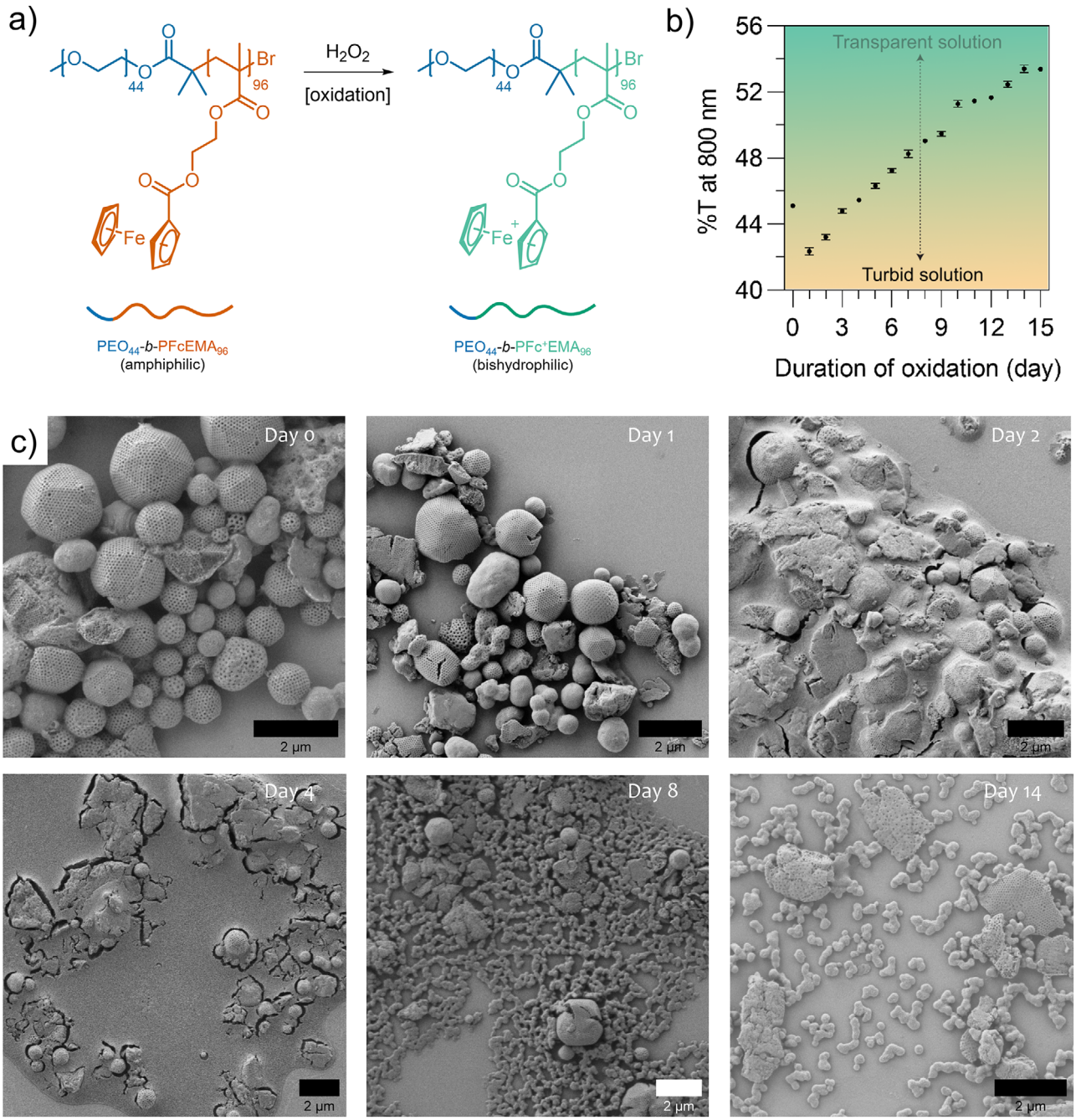

Figure 6. Oxidative dissolution of PCs. a) Amphiphilic PEO_{44}-*b*-PFcEMA$_{96}$ undergoes oxidation into bishydrophilic PEO_{44}-*b*-PFc$^+$EMA$_{96}$ in the presence of H_2O_2. b) Turbidity plot showing changes in the opacity/transparency of a PC dispersion after incubation with 100 mM H_2O_2. c) SEM image series of the same sample after H_2O_2 addition and over time as indicated.

4. Experimental Section

Materials: All chemicals were purchased from Sigma–Aldrich and used as received unless otherwise mentioned. Solvents were of analytical grade. TEM grids (400 mesh, carbon-coated copper grids) and silicon wafer (10 × 10 mm diced) were purchased from Ted Pella Inc. The rhodamine B-labelled β-cyclodextrin derivative, heptakis(6-dodecylthio-2-oligo(ethylenoxide))-rhodamine-β-CD was synthesized in ref. [47] Water (resistivity = 18.2 MΩ cm) used for experiments was obtained from a MilliQ Integral Water Purification System.

Self-Assembly of Cubosomes from PEO_{44}-b-PFcEMA$_{96}$: In a typical experiment, a stock solution of PEO_{44}-*b*-PFcEMA$_{96}$ in THF with a concentration of 10 g L^{-1} was first prepared. To ensure complete dissolution of the BCP, the solution was stirred at room temperature for at least 1 h and filtered through a 0.45 µm syringe filter before use. To initiate self-assembly, 500 µL of the stock solution was transferred into a dialysis tube with a MWCO of 14 kDa (pre-washed with water followed by THF, and

then dried gently with a stream of air) and dialyzed against water. The dialysis medium was exchanged at least 4 times over the course of 24 h. After dialysis, the cloudy yellow suspension was collected and centrifuged at 3000 rpm for 2 min. The supernatant was removed with a pipette, and the sediment redispersed in water to yield an aqueous suspension of PEO_{44}-*b*-$PFcEMA_{96}$ PCs.

Template Infiltration and Calcination to Iron Oxide Decorated SiO_2-Cubosomes: In a typical experiment, 500 µL of 10 g L^{-1} cubosome dispersion was centrifuged at 4000 rpm (5 min) and redispersed in a TEOS sol composed of 500 µL of 1M HCl and 143 µL of tetraethyl orthosilicate (TEOS). The mixture was stirred at 60 rpm on an orbital shaker for 2 h before being centrifuged at 4000 rpm (5 min) to sediment the TEOS sol-impregnated cubosomes. A pipette was then used to carefully remove the excess TEOS sol. The sediment was redispersed in minimal amounts of water (≈10 µL), transferred onto a silicon wafer, and dried in a vacuum oven at 40 °C overnight. Calcination was subsequently carried out at 500 °C in a furnace oven (air) for 5 h to yield iron oxide-decorated SiO_2-cubosomes.

Instruments: *GPC* measurements were performed on a 1260 Infinity instrument (Polymer Standard Service, Mainz) equipped with three PSS SDV columns (pore sizes 10^6, 10^5, and 10^3 Å) using HPLC-grade THF as the eluent at a flow rate of 1.0 mL min^{-1} at 40 °C (column oven TCC6000) and a refractive index detector. A narrow-molecular-weight PS standard kit (Polymer Standard Service, Mainz) was used for calibration. *NMR* was done on an Ultrashield 300 MHz spectrometer from Bruker. The samples were measured in $CDCl_3$. *SEM images* were acquired on a Zeiss CrossBeam 340 using the following settings: i) detector mode: SESI, ii) EHT = 1.00 kV, iii) working distance (WD) = 5.0 mm. Samples were typically prepared by drop-casting 10 µL of 5 g L^{-1} cubosome solution onto a silicon wafer, followed by air-drying overnight. A 10-nm Au layer was sputtered over the sample prior to imaging. *TEM measurements* were done on a JEOL 2200FS TEM operating at an accelerating voltage of 200 kV and equipped with a Gatan Ultra-Scan 1000XP CCD. TEM samples were prepared by placing a 10 µL droplet of cubosome solution (0.1 g L^{-1}) onto a carbon-coated copper grid (400 mesh size) and then evaporating the droplet slowly under ambient conditions. No staining was used. Sectioning of PEO-*b*-PFcEMA microparticles was done by first embedding freeze-dried microparticles in 3D Rapid Resin CLEAR 3DR3582C followed by polymerization under UV light (λ = 365 nm). Ultrathin cross-sections were obtained using a Reichert/Leica Ultracut E ultramicrotome (Leica Microsystems, Wetzlar, Germany) equipped with a Leica diamond knife and a milliQ water-filled boat. Sectioning was performed at an inclination angle of 6° and a cutting speed of ≈1 mm s^{-1}, producing slices with a thickness of ≈90 nm. Floating sections were collected directly from the water surface and transferred onto carbon-coated copper grids for TEM analysis. *Turbidity measurements* were conducted on a Jasco V-770 UV–vis/NIR spectrophotometer using a 1-cm pathlength quartz cuvette (3 mL). Baseline correction was performed using water as a blank. *Fluorescence spectra* were obtained using a Jasco FP 8500 spectrofluorometer using a 1-cm pathlength quartz cuvette (700 µL). Samples were excited using an excitation wavelength of 510 nm, an excitation slit of 20 nm, and an emission slit of 5 nm. *Fluorescence/brightfield* images were obtained using an Olympus BX53 microscope equipped with an XC10 Color Camera, 60x/1.25NA oil objective, and a mercury lamp. Samples were prepared by sandwiching a 30 µL droplet of RhoB-βCD-complexed cubosome solution between two coverslips sealed with high-vacuum grease. Samples were excited with a TRITC filter cube.

Supporting Information

Supporting Information is available from the Wiley Online Library or from the author.

Acknowledgements

C.K.W. is grateful to the Alexander von Humboldt Foundation for a Humboldt Research Fellowship. C.C. is grateful for financial support from the China Scholarship Council. A.H.G. acknowledges funding from the German Research Foundation (DFG, project number 526222003). RhoB-βCD was kindly provided by the group of Prof. Bart Jan Ravoo from the University of Münster.

Open access funding enabled and organized by Projekt DEAL.

Conflict of Interest

The authors declare no conflict of interest

Data Availability Statement

The data that support the findings of this study are available from the corresponding author upon reasonable request.

Keywords

block copolymers, colloids, liquid-liquid phase separation, mesoporous particles, RedOx response, self-assembly

Received: August 27, 2025
Revised: October 7, 2025
Published online: October 15, 2025

[1] Y. Mai, A. Eisenberg, *Chem. Soc. Rev.* **2012**, *41*, 5969.
[2] Y. La, C. Park, T. J. Shin, S. H. Joo, S. Kang, K. T. Kim, *Nat. Chem.* **2014**, *6*, 534.
[3] Z. Lin, S. Liu, W. Mao, H. Tian, N. Wang, N. Zhang, F. Tian, L. Han, X. Feng, Y. Mai, *Angew. Chemie – Int. Ed.* **2017**, *56*, 7135.
[4] X. Lyu, A. Xiao, W. Zhang, P. Hou, K. Gu, Z. Tang, H. Pan, F. Wu, Z. Shen, X. H. Fan, *Angew. Chemie – Int. Ed.* **2018**, *57*, 10132.
[5] C. K. Wong, M. Heidelmann, M. Dulle, X. Qiang, S. Förster, M. H. Stenzel, A. H. Gröschel, *J. Am. Chem. Soc.* **2020**, *142*, 10989.
[6] S. Ha, Y. La, K. T. Kim, *Acc. Chem. Res.* **2020**, *53*, 620.
[7] C. K. Wong, X. Qiang, A. H. E. Müller, A. H. Gröschel, *Prog. Polym. Sci.* **2020**, *102*, 101211.
[8] A. H. Gröschel, T. Gröschel, S. Azhdari, M. Schumacher, H. Chen, *ACS Nano* **2023**, *17*, 16069.
[9] C. Li, Q. Li, Y. V. Kaneti, D. Hou, Y. Yamauchi, Y. Mai, *Chem. Soc. Rev.* **2020**, *49*, 4681.
[10] H. Chen, M. H. Li, *Macromol. Rapid Commun.* **2021**, *42*, 2100194.
[11] L. Xiang, Q. Li, C. Li, Q. Yang, F. Xu, Y. Mai, *Adv. Mater.* **2023**, *35*, 2207684.
[12] T. H. An, Y. La, A. Cho, M. G. Jeong, T. J. Shin, C. Park, K. T. Kim, *ACS Nano* **2015**, *9*, 3084.
[13] Y. La, T. H. An, T. J. Shin, C. Park, K. T. Kim, *Angew. Chemie – Int. Ed.* **2015**, *54*, 10483.
[14] Y. La, J. Song, M. G. Jeong, A. Cho, S.-M. Jin, E. Lee, K. T. Kim, *Nat. Commun.* **2018**, *9*, 5327.
[15] H. Ma, K. T. Kim, *Macromolecules* **2020**, *53*, 711.
[16] Z. Lin, J. Zhou, C. Cortez-Jugo, Y. Han, Y. Ma, S. Pan, E. Hanssen, J. J. Richardson, F. Caruso, *J. Am. Chem. Soc.* **2020**, *142*, 335.
[17] L. Xiang, S. Yuan, F. Wang, Z. Xu, X. Li, F. Tian, L. Wu, W. Yu, Y. Mai, *J. Am. Chem. Soc.* **2022**, *144*, 15497.
[18] C. Li, Y. Pan, T. Xiao, L. Xiang, Q. Li, F. Tian, I. Manners, Y. Mai, *Angew. Chemie* **2023**, *135*, 202215985.
[19] Y. Liu, Q. Zhou, H. Yu, Q. Yang, M. Wang, C. Huang, L. Xiang, C. Li, T. Heine, G. Hu, S. Wang, X. Feng, Y. Mai, *Angew. Chemie – Int. Ed.* **2024**, *63*, 202400985.
[20] H. Lee, D. G. Kim, H. Ma, K. T. Kim, *Chem. Commun.* **2020**, *56*, 14059.

[21] W. Xie, X. Huang, C. Zhu, F. Jiang, Y. Deng, B. Yu, L. Wu, Q. Yue, Y. Deng, *Adv. Mater.* **2024**, *36*, 2313920.
[22] Q. Yang, Y. Liu, L. Xiang, J. Zhang, Y. Yin, F. Xu, Y. Mai, *Chem. Commun.* **2023**, *59*, 4742.
[23] Y. Pan, Y. Xin, Y. Li, Z. Xu, C. Tang, X. Liu, Y. Yin, J. Zhang, F. Xu, C. Li, Y. Mai, *ACS Nano* **2023**, *17*, 23850.
[24] Z. Xu, T. Xiao, Y. Li, Y. Pan, C. Li, P. Liu, Q. Xu, F. Tian, L. Wu, F. Xu, Y. Mai, *Adv. Mater.* **2025**, *37*, 2416204.
[25] L. Xiang, Q. Xu, H. Zhang, S. Geng, R. Cui, T. Xiao, P. Chen, L. Wu, W. Yu, H. Peng, Y. Mai, H. Sun, *Angew. Chemie – Int. Ed.* **2023**, *62*, 202312001.
[26] L. Xiang, C. Tang, Z. Xu, F. Xu, C. Li, Y. Mai, *Accounts Mater. Res.* **2025**, *6*, 939.
[27] H. Yu, X. Qiu, S. P. Nunes, K. V. Peinemann, *Nat. Commun.* **2014**, *5*, 4110.
[28] Q. Zhang, M. Lu, H. Wu, L. Zhang, X. Feng, Z. Jin, *Langmuir* **2022**, *38*, 12441.
[29] V. Wang, S. Ha, J. Kim, K. T. Kim, *Giant* **2023**, *15*, 100178.
[30] H. Chen, Y. Fan, N. Zhang, S. Trépout, B. Ptissam, A. Brûlet, B. Z. Tang, M. H. Li, *Chem. Sci.* **2021**, *12*, 5495.
[31] J. H. Kwon, J. Kim, K. T. Kim, *Polym. Chem.* **2021**, *12*, 2701.
[32] B. Fan, J. Wan, J. Zhai, X. Chen, S. H. Thang, *ACS Nano* **2021**, *15*, 4688.
[33] H. Chen, M. Schumacher, A. Ianiro, T. J. Stank, N. Janoszka, C. Chen, S. Azhdari, T. Hellweg, A. H. Gröschel, *J. Am. Chem. Soc.* **2024**, *146*, 14776.
[34] S. Azhdari, J. Linders, D. Coban, T. J. Stank, C. Dargel, H. Gojzewski, T. Hellweg, A. H. Gröschel, F. R. Wurm, *Adv. Mater.* **2024**, *36*, 2406831.
[35] M. Schumacher, M. Foith, M. Trömer, N. Tänzer, S. Rosenfeldt, M. Retsch, A. H. Gröschel, *Macromol. Rapid Commun.* **2025**, *46*, 2400633.
[36] M. Schumacher, N. Tänzer, M. G. Braun, M. Trömer, G. Quintieri, M. Goel, M. Heidelmann, A. H. Gröschel, *Small Sci* **2024**, *4*, 2400274.
[37] D. Astruc, *Eur. J. Inorg. Chem.* **2017**, *2017*, 6.
[38] C. G. Hardy, L. Ren, T. C. Tamboue, C. Tang, *J. Polym. Sci. Part A Polym. Chem.* **2011**, *49*, 1409.
[39] S. Alberti, A. Gladfelter, T. Mittag, *Cell* **2019**, *176*, 419.
[40] M. Mazurowski, M. Gallei, J. Li, H. Didzoleit, B. Stühn, M. Rehahn, *Macromolecules* **2012**, *45*, 8970.
[41] C. G. Hardy, L. Ren, S. Ma, C. Tang, *Chem. Commun.* **2013**, *49*, 4373.
[42] D. Demurtas, P. Guichard, I. Martiel, R. Mezzenga, C. Hébert, L. Sagalowicz, *Nat. Commun.* **2015**, *6*, 8915.
[43] A. Harada, S. Takahashi, *J. Chem. Soc. Chem. Commun.* **1984**, *10*, 645.
[44] L. Peng, A. Feng, M. Huo, J. Yuan, *Chem. Commun.* **2014**, *50*, 13005.
[45] F. Szillat, B. V. K. J. Schmidt, A. Hubert, C. Barner-Kowollik, H. Ritter, *Macromol. Rapid Commun.* **2014**, *35*, 1293.
[46] M. Nakahata, Y. Takashima, H. Yamaguchi, A. Harada, *Nat. Commun.* **2011**, *2*, 511.
[47] O. Roling, C. Wendeln, U. Kauscher, P. Seelheim, H. J. Galla, B. J. Ravoo, *Langmuir* **2013**, *29*, 10174.
[48] J. Tan, H. Li, X. Hu, R. Abdullah, S. Xie, L. Zhang, M. Zhao, Q. Luo, Y. Li, Z. Sun, Q. Yuan, W. Tan, *Chem* **2019**, *5*, 1775.